Determination of product population and alignment using laser-induced fluorescence[a)]

Chris H. Greene

Department of Physics and Astronomy, Louisiana State University, Baton Rouge, Louisiana 70803

Richard N. Zare[b)]

Department of Chemistry, Stanford University, Stanford, California 94305
(Received 20 January 1983; accepted 16 February 1983)

For collision systems having axial symmetry, the anisotropy of the laser-induced fluorescence is given explicitly in terms of the zeroth, second, and fourth rank moments of the angular momentum distribution, which, respectively, are proportional to the population, the quadrupole alignment, and hexadecapole alignment of the product internal state under study. Expressions are presented for determining these three quantities from the dependence of the fluorescence intensity on the polarizations of the absorbed and detected photons. Results are presented for an arbitrary excitation-detection geometry which is then specialized to the commonly occurring cases where the direction of fluorescence detection is at right angles to the axis of cylindrical symmetry and the direction of the incoming light beam is either along the axis of cylindrical symmetry or at right angles to it and to the fluorescence detection direction. The approach of these expressions to the high-J limit is considered. The effect of nuclear spin on the fluorescence intensity is analyzed and the extent of depolarization is shown to be unimportant for large J. The use of angular momentum recoupling algebra permits the geometrical and dynamical aspects of this problem to be completely disentangled.

I. INTRODUCTION

A powerful technique for analyzing fragments produced by a reactive collision is the observation of chemiluminescence. Of course, the fragments must be born in an excited state. A common goal is to extract relative populations of internal states from the chemiluminescence intensity distribution. As is well known, this procedure requires not only the measurement of accurate intensities but also a knowledge of the polarization of the emitted light. A classic paper by Fano and Macek (FM)[1] showed how the light intensity depends on the detection geometry and on the collision dynamics. In particular, one can determine three kinds of quantities: the population and elements of the first and second rank multipole moments of the total fragment angular momentum, called the orientation and the alignment, respectively. Recently, the FM[1] treatment of fluorescence polarization has been discussed by Greene and Zare (GZ)[2] in the context of photofragmentation.

Frequently reactive collisions of interest do not yield excited fragments suitable for study by observation of chemiluminescence. However, it is still possible to learn about the collision dynamics through the technique of laser-induced fluorescence (LIF) in which one detects the emission from a collision fragment following laser excitation.[3–5] Once again in analogy to chemiluminescence, relative internal state populations cannot be extracted from the intensity without knowledge of the directions and polarizations of the incoming and outgoing photons. This last aspect is often neglected in relative population measurements, but it can be important and is the subject of this paper. The LIF technique permits the determination of five kinds of quantities: the population, and the elements of the first and third rank multipoles (the dipole and octopole orientation) and the second and fourth rank multipoles (the quadrupole and hexadecapole alignment). This problem has been considered in complete generality by Fano and Racah (FR),[6] and more recently by Case, McClelland, and Herschbach (CMH).[7] Unfortunately these studies have not been easily accessible to most experimentalists, as the final results, expressed in density matrix notation, are quite complicated and even intimidating. Our aim here is to simplify as much as possible the theory of LIF and to specialize it to commonly occurring experimental geometries. We consider only *axially symmetric* systems in which the colliding particles have no helicity (no handedness). These include beam-gas collisions, for which the beam axis serves as the symmetry axis, and beam–beam collisions, for which the initial relative velocity vector serves as the symmetry axis. In the latter case, this requires that all products are probed with a probability independent of their scattering direction. Also encompassed are photofragmentation experiments using linearly polarized or unpolarized incident light, with symmetry axes lying along the polarization vector or the photon propagation vector, respectively, although for such experiments the hexadecapole alignment must vanish for an electric dipole process. Of course, electron beam and ion beam excitation/fragmentation also belong to this class of experiments, but will generally have a nonzero hexadecapole alignment. The cylindrical symmetry in each of the above cases would be lost, however, if the angular distribution of a fragment is simultaneous-

[a)]Support by the National Science Foundation is gratefully acknowledged.

[b)]R. N. Z. gratefully acknowledges support through the Shell Distinguished Chairs Program, funded by the Shell Companies Foundation, Inc.

ly observed.[7] These restrictions exclude the odd rank multipole moments, i.e., only the population and the axially symmetric quadrupole and hexadecapole alignment, denoted by $\mathcal{A}_0^{(2)}$ and $\mathcal{A}_0^{(4)}$, can be measured. The alignment parameters $\mathcal{A}_0^{(2)}$ and $\mathcal{A}_0^{(4)}$ contain the complete dynamical information about the reaction product (or fragment) prepared in the initial state $|i\rangle$ with the angular momentum vector $\mathbf{J}_i$. This is all that can be learned from the variation of the laser-induced fluorescence signal with the polarization of the detected and absorbed photons for a system having axial symmetry. Let z be chosen to be along the axis of cylindrical symmetry. Then, as will be shown, $\mathcal{A}_0^{(2)}$ is proportional to $P_2(\hat{J}_i \cdot \hat{z})$ for all J_i while $\mathcal{A}_0^{(4)}$ rapidly becomes proportional to $P_4(\hat{J}_i \cdot \hat{z})$ as J_i increases. Here the superscript caret represents a unit vector and P_n is a Legendre polynomial of order n. Thus, the $\mathcal{A}_0^{(2)}$ and $\mathcal{A}_0^{(4)}$ correspond to the classical quadrupole and hexadecapole moments of the angular distribution of $\mathbf{J}_i$ vectors. Consequently, the measured alignment parameters can be readily interpreted qualitatively in terms of the shape of the product (fragment) angular momentum distribution.

The spatial alignment of fragment angular momentum excited by a collision often reflects the reaction physics sharply.[8,9] Accordingly, a measurement of this detailed information permits a telling comparison to be made with dynamical models—even more so than does a state-to-state reaction cross section. Fragment alignment influences the subsequent scattering of reaction products.[10–12] Moreover, even if the alignment is not of interest, it is essential to know precisely how it can affect a measurement of product population.

We emphasize at the outset that the formulation presented here is valid only when the intensity of the incident laser does not cause appreciable optical pumping[13] and saturation effects.[14] Thus, we consider a regime in which the pumping process is not so strong as to perturb the population or alignment of the ensemble, or to induce appreciable stimulated emission and absorption cycles. This may require extrapolation of measured LIF intensities to the low-power limit both for the case of pulsed and cw dye lasers.

The remainder of this paper has been divided into two parts, of which Sec. II is intended as a guide for the experimentalist and Sec. III presents a derivation of the key results found in Sec. II. This derivation is modeled after the FM[1] treatment of fluorescence polarization, and does not make use of density matrices. We find that the intensity of LIF can be decomposed into separate dynamical and geometrical factors. This explicit separation is presented in Sec. II for two convenient and traditional excitation-detection geometries in which the fluorescence detection direction is at right angles to the axis of cylindrical symmetry; an Appendix considers more general geometries. The LIF intensity simplifies greatly in the limit of large product angular momenta, but we show that the approach to this limit may be slow in many cases, as noted previously by CMH.[7] Section II also discusses how to use the LIF intensity expression to design experiments for measuring the product population and/or alignment.

An axially symmetric system has in general $[J_i]$ multipole moments of even rank. Yet the LIF technique using linearly polarized excitation and detection can only determine the two lowest moments, the quadrupole and hexadecapole alignment. This may seem rather disappointing at first. However, it can be advantageous to study initially such a coarse measure of the dynamics, since the predictions of many dynamical models can be readily distinguished even at this level.

II. DEPENDENCE OF LIF INTENSITY ON THE INCIDENT AND EMITTED LIGHT DIRECTIONS AND POLARIZATIONS

A. General intensity formula for axially symmetric systems

The primary aim of this section is to present a theoretical expression for the intensity of laser-induced fluorescence in terms of two rather different types of quantities, one *geometrical*, the other *dynamical*. The first or geometrical type consists of standard parameters depending only on the angular momentum quantum numbers of the initial (J_i), excited (J_e), and final (J_f) states of the reaction product and on the directions and polarizations of the incident and emitted light. This factor reflects only the dipole nature of the absorption–emission process and the excitation-detection geometry employed. The second or dynamical type consists of three parameters representing the monopole, quadrupole, and hexadecapole moments of the angular momentum distribution in the initial state $|i\rangle$. The monopole moment expresses the total number (occupation number) of product species in the initial state while the quadrupole and hexadecapole moments describe the nature of the alignment of this state. These dynamical parameters tell us about the reaction process that formed the product species; they exhaust the information about the reaction that can be determined using LIF. It is the goal of LIF studies to devise a procedure for extracting these three dynamical quantities from measurements of the LIF intensity.

Figure 1 shows the energetics of the LIF process. The fluorescence probe beam pumps the initial state $|i\rangle$ to an excited state $|e\rangle$, which subsequently emits radiation as a transition is made to the final state $|f\rangle$. Both $|i\rangle$ and $|f\rangle$ lie below $|e\rangle$ but the energy level ordering of $|i\rangle$ and $|f\rangle$ does not matter. It is also possible that $|i\rangle$ and $|f\rangle$ are the same state but this fact is also irrelevant. Dipole selection rules require the angular momentum quantum numbers to satisfy the relations $J_e - J_i = 0, \pm 1$ and $J_f - J_e = 0, \pm 1$ with the additional condition that $J_i + J_e \neq 0$ and $J_e + J_f \neq 0$. Then the intensity of

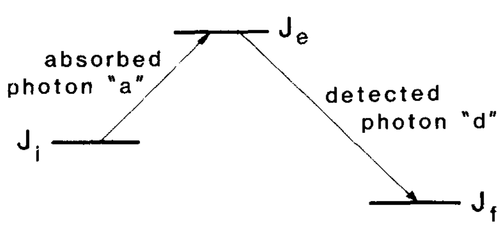

FIG. 1. The laser-induced fluorescence process.

fluorescence from a cylindrically symmetric ensemble can be written as a sum of products of molecular alignment parameters $\mathcal{A}$, excitation-detection geometrical factors ϵ, and angular momentum coupling factors ω:

$$I = CS \sum_{k_d, k_a, k} \mathcal{A}_0^{(k)} \epsilon(k_d, k_a, k, 0; \Omega) \times \omega(k_d, k_a, k; J_i, J_e, J_f) \ . \tag{1}$$

The remainder of this section discusses the meaning of this formula, which can be derived from Eq. (42) specialized to $q=0$ (see Sec. III), and offers suggestions on how to use it for designing and interpreting LIF experiments.

The indices k_d and k_a are the multipole moments of the detected and absorbed photons, respectively, while the index k represents the multipole moment of the combined resonance fluorescence process. The multiple summations over k_d, k_a, and k appearing in Eq. (1) are really rather simple because these quantum numbers are restricted to low values owing to the dipole nature of the absorption and emission steps of the resonance fluorescence process: $k_d = 0, 2$; $k_a = 0, 2$; and $k = 0, 2, 4$. Also, the relation $\mathbf{k}_d + \mathbf{k}_a = \mathbf{k}$ holds in the sense of angular momentum addition. Consequently there are a total of only six nonvanishing terms in the summation shown in Eq. (1). The constant C is proportional to the total population of the initial state $|i\rangle$, while S is the product of the line strengths for the two transitions $i \to e$ and $e \to f$. In terms of reduced dipole matrix elements

$$S = |(J_f \| r^{(1)} \| J_e)(J_e \| r^{(1)} \| J_i)|^2 \ . \tag{2}$$

The terms inside the summation are more critical for our discussion.

The $\mathcal{A}_0^{(k)}$ are mean values of the monopole, quadrupole, and hexadecapole combinations of the angular momentum operators $\mathbf{J}$ operating on the initial state:

$$\mathcal{A}_0^{(0)} = 1 \ , \tag{3}$$

$$\mathcal{A}_0^{(2)} = \left\langle\left(J_i \left| \frac{3J_z^2 - \mathbf{J}^2}{\mathbf{J}^2} \right| J_i \right)\right\rangle \ , \tag{4}$$

$$\mathcal{A}_0^{(4)} = \left\langle\left(J_i \left| \frac{3\mathbf{J}^4 - 6\mathbf{J}^2 - 30J_z^2\mathbf{J}^2 + 25J_z^2 + 35J_z^4}{8\mathbf{J}^4} \right| J_i \right)\right\rangle \ . \tag{5}$$

The alignment parameters $\mathcal{A}_0^{(2)}$ and $\mathcal{A}_0^{(4)}$ represent the desired dynamical information about the reaction which prepared the initial state $|i\rangle$. At all J_i $\mathcal{A}_0^{(2)}$ may be written as the expectation value of a Legendre polynomial $\mathcal{A}_0^{(2)} = 2\langle P_2(\hat{J}\cdot\hat{z})\rangle$ but the corresponding relation $\mathcal{A}_0^{(4)} = \langle P_4(\hat{J}\cdot\hat{z})\rangle$ is only valid[2] in the limit $J_i \to \infty$. However, this limit is approached very rapidly, as will be shown below. The alignment parameters lie in general within the respective ranges

$$-1 \le \mathcal{A}_0^{(2)} \le 2 \tag{6}$$

and

$$-\tfrac{3}{7} \le \mathcal{A}_0^{(4)} \le 1 \ . \tag{7}$$

Moreover, if the alignment is created by photofragmentation, then $\mathcal{A}_0^{(4)} = 0$ and $\mathcal{A}_0^{(2)}$ lies between -1 and $\frac{4}{5}$ (which becomes $-\frac{2}{5}$ and $\frac{4}{5}$ in the limit of large J_i). Actually, for any fixed J_i all these limits are more restrictive than Eqs. (6) and (7), particularly for low J_i values.

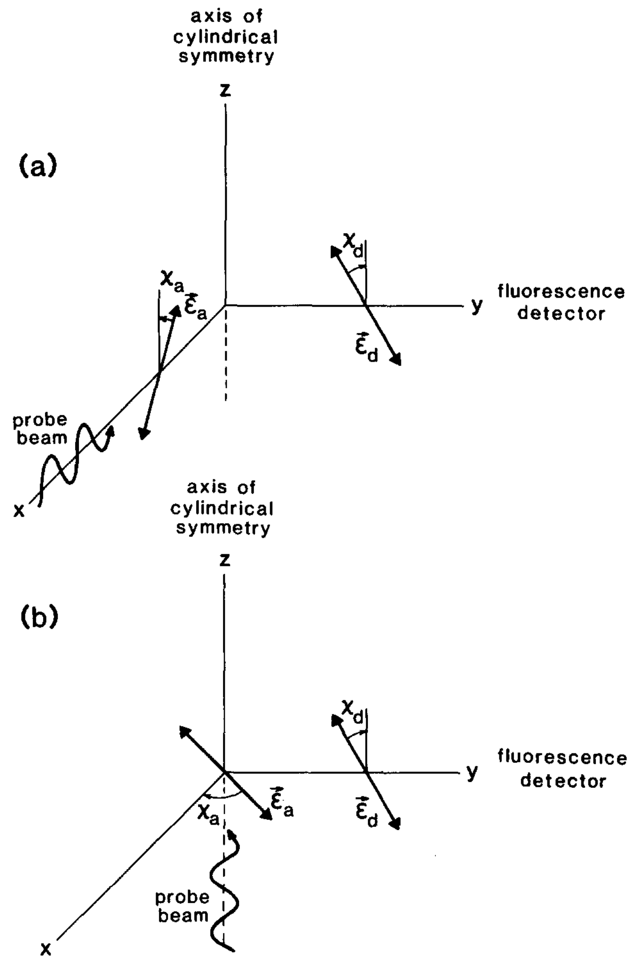

FIG. 2. Two traditional excitation-detection configurations: (a) the mutually orthogonal geometry; and (b) the coaxially probed geometry. In each case the direction of cylindrical symmetry lies along z and the direction of fluorescence detection lies along y. The angles χ_a and χ_d define the directions of the linear polarization vectors ϵ_a and ϵ_d of the absorbed and detected photons, as shown.

The remaining factors ϵ and ω are purely geometrical. The $\epsilon(k_d, k_a, k, 0; \Omega)$ are "polarization tensors" which contain all relevant information regarding the spatial locations and linear polarizer orientations of the incident laser light source and of the fluorescence detector. There are two convenient excitation-detection geometries, shown in Fig. 2. In one of these the excitation direction, the detection direction, and the direction of cylindrical symmetry are mutually orthogonal [Fig. 2(a)]. In the other, the excitation direction and the direction of cylindrical symmetry coincide while the detection direction is at right angles [Fig. 2(b)]. We call the first configuration the *mutually orthogonal geometry* and the second the *coaxially probed geometry*. The corresponding polarization tensors are listed in Table I. The results of Table I also apply to unpolarized excitation and/or detection. In each appropriate case one simply adds the $\chi = 0°$ and $\chi = 90°$ values of ϵ.

TABLE I. Polarization tensors for an axially symmetric system for two common excitation-detection configurations.

$\epsilon(k_d, k_a, k, 0; \Omega)$	Explicit form
	Mutually orthogonal geometry
$\epsilon(0,0,0,0;\Omega)$	$\frac{1}{3}$
$\epsilon(2,2,0,0;\Omega)$	$\frac{1}{2\sqrt{5}}[\frac{4}{3}P_2(\cos\chi_d)P_2(\cos\chi_a)-\sin^2\chi_d\sin^2\chi_a]$
$\epsilon(2,0,2,0;\Omega)$	$-\frac{2}{3\sqrt{2}}P_2(\cos\chi_d)$
$\epsilon(0,2,2,0;\Omega)$	$-\frac{2}{3\sqrt{2}}P_2(\cos\chi_a)$
$\epsilon(2,2,2,0;\Omega)$	$-\frac{1}{\sqrt{14}}[\frac{4}{3}P_2(\cos\chi_d)P_2(\cos\chi_a)+\sin^2\chi_d\sin^2\chi_a]$
$\epsilon(2,2,4,0;\Omega)$	$\frac{1}{2\sqrt{70}}[8P_2(\cos\chi_d)P_2(\cos\chi_a)-\sin^2\chi_d\sin^2\chi_a]$
	Coaxially probed geometry
$\epsilon(0,0,0,0;\Omega)$	$\frac{1}{3}$
$\epsilon(2,2,0,0;\Omega)$	$-\frac{1}{2\sqrt{5}}[\frac{2}{3}P_2(\cos\chi_d)-\sin^2\chi_d\cos 2\chi_a]$
$\epsilon(2,0,2,0;\Omega)$	$-\frac{2}{3\sqrt{2}}P_2(\cos\chi_d)$
$\epsilon(0,2,2,0;\Omega)$	$\frac{1}{3\sqrt{2}}$
$\epsilon(2,2,2,0;\Omega)$	$\frac{1}{\sqrt{14}}[\frac{2}{3}P_2(\cos\chi_d)+\sin^2\chi_d\cos 2\chi_a]$
$\epsilon(2,2,4,0;\Omega)$	$-\frac{1}{2\sqrt{70}}[4P_2(\cos\chi_d)-\sin^2\chi_d\cos 2\chi_a]$

The more general forms of $\epsilon(k_d, k_a, k, 0; \Omega)$ for an arbitrary excitation-detection geometry are given in the Appendix.

Most experiments are carried out with the polarization vector of the probe beam either along or perpendicular to the collision symmetry axis (the z axis) while at the same time the fluorescence is detected at right angles (along the y axis) with its polarization analyzer set to accept polarized emission either along the collision symmetry axis (the z axis) or perpendicular to it (along the x axis). As a convenience, Table II lists the values of ϵ for each excitation-detection geometry. Notice that only five distinct cases result (case three = case five ≡ case seven, and case four = case six) since it is the relative spatial orientations of the polarization vectors of the absorbed and detected photons with respect to the fluorescence detection direction which determines the value of ϵ.

Finally, the remaining factor $\omega(k_d, k_a, k; J_i, J_e, J_f)$ contains the sole dependence of the LIF intensity on the angular momenta of the initial, excited, and final states. As discussed in Sec. III, ω results from recoupling these angular momenta using the well known Wigner–Racah algebra machinery.[6] The resulting expressions contain Wigner $6j$ and $9j$ symbols, which may appear fierce to the uninitiated, but in reality are nothing but fractional numbers that can be computed according to well-defined algorithms.[15,16] Explicitly, we find

$$\omega(k_d, k_a, k; J_i, J_e, J_f) = b^{(k)}(J_i) h(k_d, k_a, k; J_i, J_e, J_f) , \tag{8}$$

where

$$h(k_d, k_a, k; J_i, J_e, J_f) = (-1)^{J_e+J_f+1}(2k_d+1)^{1/2}(2k_a+1)^{1/2}(2k+1)^{1/2}\begin{Bmatrix} J_e & J_e & k_d \\ 1 & 1 & J_f \end{Bmatrix}\begin{Bmatrix} J_e & 1 & J_i \\ J_e & 1 & J_i \\ k_d & k_a & k \end{Bmatrix} \tag{9}$$

and the rescaling factors $b^{(k)}(J_i)$ are given by

$$b^{(0)}(J_i) = (2J_i+1)^{-1/2} , \tag{10}$$

$$b^{(2)}(J_i) = \left[\frac{J_i(J_i+1)}{(2J_i+3)(2J_i+1)(2J_i-1)}\right]^{1/2} , \tag{11}$$

$$b^{(4)}(J_i) = \frac{4J_i^2(J_i+1)^2}{[(J_i+2)(J_i+1)J_i(J_i-1)(2J_i+5)(2J_i+3)(2J_i+1)(2J_i-1)(2J_i-3)]^{1/2}} . \tag{12}$$

The physical origin of these various factors is discussed in Sec. III. The crucial point here is that they are just real numbers which can be routinely evaluated for any particular transition of interest, and which acquire a simple form in the high-J_i limit.

For $0 < J_i < \frac{1}{2}k$ the denominator of the factor $b^{(k)}(J_i)$ vanishes; however, for the same condition both $\mathcal{A}^{(k)}$ and $h(k_d, k_a, k; J_i, J_e, J_f)$ are also identically zero. Hence in evaluating Eq. (1) all terms with $k > 2J_i$ should be omitted.

An important special case of Eq. (1) is an isotropic distribution of product species. Then $\mathcal{A}^{(k)} = 0$ for all $k > 0$. The $k = 0$ terms of Eq. (1) can be readily evaluated since the $9j$ symbols have at least one vanishing argument. Equation (1) becomes

$$I = CS\left[\frac{1}{9(2J_i+1)(2J_e+1)} + \frac{2(-1)^{J_i-J_f}}{3(2J_i+1)} \times \begin{Bmatrix} J_e & J_e & 2 \\ 1 & 1 & J_f \end{Bmatrix}\begin{Bmatrix} J_e & J_e & 2 \\ 1 & 1 & J_i \end{Bmatrix} P_2(\cos\chi_{ad})\right] , \tag{13}$$

where $\cos\chi_{ad}$, the cosine of the angle between the absorption and detection polarization axes, is simply $\cos\chi_d\cos\chi_a$ for the geometry of Fig. 2(a) and $\sin\chi_d\cos\chi_a$ for Fig. 2(b). As Eq. (13) shows, the laser-induced fluorescence signal from an isotropic distribution can be polarized, i.e., depends only on the angle between

TABLE II. Values of the polarization tensors of a cylindrically symmetric system for special settings of the polarization vector ϵ of the absorbed and detected photons.

	$\epsilon(k_d, k_a, k, 0; \Omega) \equiv (k_d, k_a, k)$					
Case	(0, 0, 0)	(2, 2, 0)	(2, 0, 2)	(0, 2, 2)	(2, 2, 2)	(2, 2, 4)
Mutually orthogonal geometry						
1. $\epsilon_a \parallel \hat{z}$; $\epsilon_d \parallel \hat{z}$	$\frac{1}{3}$	$\frac{2}{3\sqrt{5}}$	$-\frac{2}{3\sqrt{2}}$	$-\frac{2}{3\sqrt{2}}$	$-\frac{4}{3\sqrt{14}}$	$\frac{4}{\sqrt{70}}$
2. $\epsilon_a \parallel \hat{z}$; $\epsilon_d \parallel \hat{x}$	$\frac{1}{3}$	$-\frac{1}{3\sqrt{5}}$	$\frac{1}{3\sqrt{2}}$	$-\frac{2}{3\sqrt{2}}$	$\frac{2}{3\sqrt{14}}$	$-\frac{2}{\sqrt{70}}$
3. $\epsilon_a \parallel \hat{y}$; $\epsilon_d \parallel \hat{z}$	$\frac{1}{3}$	$-\frac{1}{3\sqrt{5}}$	$-\frac{2}{3\sqrt{2}}$	$\frac{1}{3\sqrt{2}}$	$\frac{2}{3\sqrt{14}}$	$-\frac{2}{\sqrt{70}}$
4. $\epsilon_a \parallel \hat{y}$; $\epsilon_d \parallel \hat{x}$	$\frac{1}{3}$	$-\frac{1}{3\sqrt{5}}$	$\frac{1}{3\sqrt{2}}$	$\frac{1}{3\sqrt{2}}$	$-\frac{4}{3\sqrt{14}}$	$\frac{1}{2\sqrt{70}}$
Coaxially probed geometry						
5. $\epsilon_a \parallel \hat{y}$; $\epsilon_d \parallel \hat{z}$	$\frac{1}{3}$	$-\frac{1}{3\sqrt{5}}$	$-\frac{2}{3\sqrt{2}}$	$\frac{1}{3\sqrt{2}}$	$\frac{2}{3\sqrt{14}}$	$-\frac{2}{\sqrt{70}}$
6. $\epsilon_a \parallel \hat{y}$; $\epsilon_d \parallel \hat{x}$	$\frac{1}{3}$	$-\frac{1}{3\sqrt{5}}$	$\frac{1}{3\sqrt{2}}$	$\frac{1}{3\sqrt{2}}$	$-\frac{4}{3\sqrt{14}}$	$\frac{1}{2\sqrt{70}}$
7. $\epsilon_a \parallel \hat{x}$; $\epsilon_d \parallel \hat{z}$	$\frac{1}{3}$	$-\frac{1}{3\sqrt{5}}$	$-\frac{2}{3\sqrt{2}}$	$\frac{1}{3\sqrt{2}}$	$\frac{2}{3\sqrt{14}}$	$-\frac{2}{\sqrt{70}}$
8. $\epsilon_a \parallel \hat{x}$; $\epsilon_d \parallel \hat{x}$	$\frac{1}{3}$	$\frac{2}{3\sqrt{5}}$	$\frac{1}{3\sqrt{2}}$	$\frac{1}{3\sqrt{2}}$	$\frac{2}{3\sqrt{14}}$	$\frac{3}{2\sqrt{70}}$

the incident and detected polarization axes. Moreover, the degree of polarization can be high. For example, in the LIF transition $0 \rightarrow 1 \rightarrow 0$ the linear polarization of the fluorescence is 100% with respect to the polarization axis of the incident light. Equation (13) agrees with results given previously by several authors.[17–19]

B. Extraction of product alignment parameters and populations using an orthogonal excitation-detection geometry

Equations (1)–(12), in conjunction with Table I, are all that are needed to determine the population n_i, the quadrupole alignment $\mathcal{A}_0^{(2)}$, and the hexadecapole alignment $\mathcal{A}_0^{(4)}$ of a given product state $|i)$ using LIF. Next we will use these results to identify some possible experimental strategies for measuring these dynamical parameters. Unlike the more general case, all three of these quantities can be determined for an axially symmetric system by using just one setting of the excitation and detection beam directions. Moreover, only one of the polarization angles χ_d or χ_a needs to be varied while the other is held fixed. These two considerations can appreciably simplify the experimental arrangement necessary to extract n_i, $\mathcal{A}_0^{(2)}$, and $\mathcal{A}_0^{(4)}$.

1. The general case $J_i \rightarrow J_e \rightarrow J_f$

The simplest and probably most accurate method of finding them is to measure the LIF intensity for a large variety of polarizer settings (χ_d, χ_a). Using Eq. (1), a linear least squares fit then determines the three dynamical parameters CS, $\mathcal{A}_0^{(2)}$, and $\mathcal{A}_0^{(4)}$. In many cases, however, the experimentalist may be interested in a more limited set of these parameters, such as only the population or only the alignment. Then it may prove advantageous to choose more carefully only a few polarizer settings which isolate the dynamical parameters of greatest interest. The following discussion develops some of these considerations.

a. Test for product alignment. In many experiments it may be the case that product alignment is negligible so that populations can be extracted without concern for polarization. Therefore it may be desirable to test first for the presence of alignment. A simple scheme for the mutually orthogonal excitation-detection geometry is to set either χ_d or χ_a to 90°. The corresponding scheme for the coaxially probed geometry involves setting χ_a to 90°. If alignment is absent, then the LIF intensity becomes *independent* of the other polarizer setting. Thus by rotating the other polarization analyzer a simple measure is obtained for the presence of alignment. This result readily follows from symmetry considerations.[20] More generally, one can compare the LIF intensity for pairs of polarizer settings (χ_d, χ_a) such that the polarization tensor

$$\epsilon(2, 2, 0, 0; \Omega) = \frac{2}{3\sqrt{5}} P_2(\cos \chi_{ad}) \tag{14}$$

is a constant. Any change in the LIF intensity indicates that at least one of the alignment parameters $\mathcal{A}_0^{(2)}$ or $\mathcal{A}_0^{(4)}$ is nonzero. A simple method for verifying the axial symmetry of the experiment, in the coaxially probed geometry, is to set χ_d to 0°, whereby the LIF intensity must be independent of χ_a, even in the presence of alignment.

b. Determination of $\mathcal{A}_0^{(2)}$ when $\mathcal{A}_0^{(4)} \neq 0$; the magic line $M_4(\chi_d, \chi_a)$. The determination of molecular align-

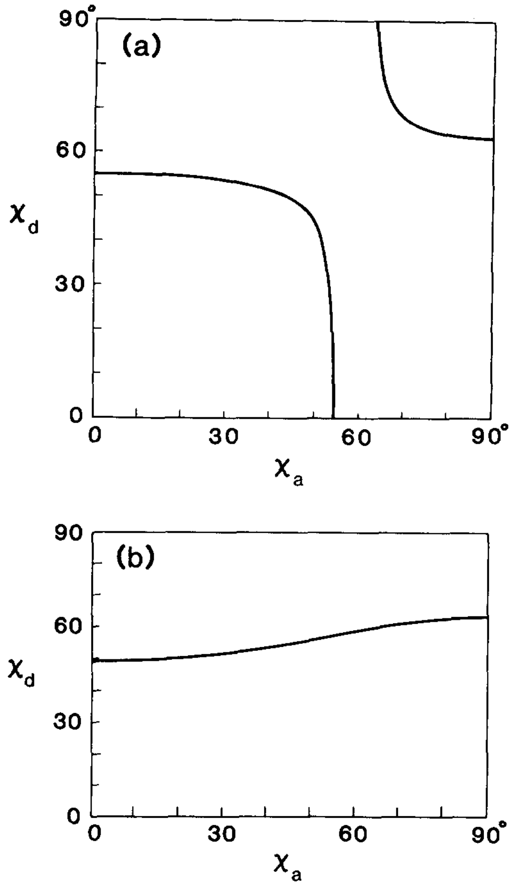

FIG. 3. The magic line $M_4(\chi_d, \chi_a)$ along which $\epsilon(2,2,4,0;\Omega)$ vanishes for (a) the mutually orthogonal and (b) the coaxially probed excitation–detection geometry. Measurements made along this line are independent of the hexadecapole alignment $\mathcal{A}_0^{(4)}$.

ment from measurements of polarized LIF is complicated by several aspects of the intensity expression (1). For one, the $\{k_d, k_a, k\}=\{2, 2, 0\}$ term in Eq. (1) implies that laser-induced fluorescence is polarized even in the absence of any product alignment [see Eq. (13) and Discussion]. A second complication in unraveling the intensity expression (1) is the simultaneous occurrence of *two* unknown alignment parameters $\mathcal{A}_0^{(2)}$ and $\mathcal{A}_0^{(4)}$. For the detection of fluorescence from axially symmetric systems, one can choose a polarization setting (the "magic angle" $\chi_d = 54.7°$) such that the intensity is independent of the alignment. In LIF probes of axially symmetric systems, it is not possible in general to find a setting (χ_d, χ_a) such that the intensity is independent of *both* $\mathcal{A}_0^{(2)}$ and $\mathcal{A}_0^{(4)}$. This difficulty can be alleviated somewhat by choosing polarizer settings such that the coefficient of one alignment parameter or the other vanishes. The simplest way to do this is to find the polarizer settings at which $\epsilon(2, 2, 4, 0; \Omega)=0$ as the LIF intensity is then *independent* of $\mathcal{A}_0^{(4)}$. These settings define a curve or magic line in the (χ_d, χ_a) plane which we denote by $M_4(\chi_d, \chi_a)$. Along M_4 the polarizer settings are the solutions of

$$\cos^2\chi_a = \frac{1+5P_2(\cos\chi_d)}{1+17P_2(\cos\chi_d)} \tag{15a}$$

and

$$\cos^2\chi_a = -6 + 4/\sin^2\chi_d \tag{15b}$$

for the mutually orthogonal geometry (15a) and the coaxially probed geometry (15b), respectively. Note that Eq. (15a) is also valid when χ_d and χ_a are interchanged, but that Eq. (15b) is not. The magic line M_4 is shown in Fig. 3. Two unconnected branches appear in Fig. 3(a), while Fig. 3(b) has but a single branch. Measurements made along these lines may prove useful when only the quadrupole alignment $\mathcal{A}_0^{(2)}$ is of interest.

The expression for the LIF intensity $I = I(\chi_d, \chi_a)$ simplifies greatly for certain settings of the excitation and detection polarizers. For example, for the mutually orthogonal geometry

$$I(0°, 54.7°) = CS\left[\frac{1}{9(2J_i+1)(2J_e+1)} - \frac{\sqrt{2}}{3}\mathcal{A}_0^{(2)}\omega(2,0,2;J_i,J_e,J_f)\right] \tag{16a}$$

and

$$I(54.7°, 0°) = CS\left[\frac{1}{9(2J_i+1)(2J_e+1)} - \frac{\sqrt{2}}{3}\mathcal{A}_0^{(2)}\omega(0,2,2;J_i,J_e,J_f)\right]. \tag{16b}$$

Equations (16a) and (16b) are but one of many examples in which $I(\chi_d, \chi_a) \neq I(\chi_a, \chi_d)$ when the product is aligned. Often these two measurements suffice to determine $\mathcal{A}_0^{(2)}$ and the population (proportional to C), except in the high-J_i limit where the coefficients $\omega(2, 0, 2; J_i, J_e, J_f)$ and $\omega(0, 2, 2; J_i, J_e, J_f)$ become equal when $(-1)^{J_i - J_f} = 1$, i.e., when $J_i - J_f$ is even.

c. Determination of $\mathcal{A}_0^{(4)}$. It would similarly prove advantageous to find a set of polarizer settings for which the intensity is independent of $\mathcal{A}_0^{(2)}$. Yet this is not straightforward owing to the presence of *three* $k=2$ terms in Eq. (1), namely $\{k_d, k_a, k\}=\{2, 0, 2\}$, $\{0, 2, 2\}$, and $\{2, 2, 2\}$. In particular, the relative contributions from each of these terms depends on the quantum numbers J_i, J_e, and J_f, so any magic line $M_2(\chi_d, \chi_a)$ for which the coefficient of $\mathcal{A}_0^{(2)}$ vanishes will clearly depend on the quantum numbers and on the structure of the absorption $(P\uparrow, Q\uparrow, R\uparrow)$ and emission $(P\downarrow, Q\downarrow, R\downarrow)$ branches. For a specific fluorescence process the relevant values of χ_d and χ_a can always be found once the factors $\omega(k_d, k_a, k; J_i, J_e, J_f)$ have been evaluated, but it will not serve our purposes to show the complicated result here.

3. The high-J_i limit

Because moderate-to-heavy molecules typically have J_i values between 10 and 100, it is of practical importance to investigate the form of the fluorescence intensity expression for $I(\chi_d, \chi_a)$ as J_i becomes large. This task is made easier by rewriting the angular momentum coefficients ω as

$$\omega(k_d, k_a, k; J_i, J_e, J_f) = N_{k_d k_a k}\gamma_{k_d k_a k}(J_i, J_e, J_f)t_{ie}(J_i, J_e)t_{ef}(J_e, J_f) \tag{17}$$

since the $\gamma_{k_d k_a k}$ become independent of J_i, J_e, and J_f as J_i becomes large. Here the parameters t_{ie} and t_{ef} contain the dependence on the absorption and emission branches according to

$$t_{ie}=\begin{cases} 1 & J_i=J_e\pm 1 \quad (P\uparrow \text{ or } R\uparrow) \\ -2 & J_i=J_e \quad (Q\uparrow) \end{cases},$$

$$t_{ef}=\begin{cases} 1 & J_e=J_f\pm 1 \quad (R\downarrow \text{ or } P\downarrow) \\ -2 & J_e=J_f \quad (Q\downarrow) \end{cases}, \tag{18}$$

and the $N_{k_d k_a k}\epsilon(k_d, k_a, k, 0;\Omega)$ take a simple form without the appearance of the square root signs in Table I. Then Eq. (1) can be rewritten for the mutually orthogonal geometry [Fig. 2(a)] as

$$I(\chi_d,\chi_a)=\frac{CS}{9(2J_i+1)(2J_e+1)}\{1+\gamma_{220}t_{ie}t_{ef}[\tfrac{4}{3}P_2(\cos\chi_d)P_2(\cos\chi_a)-\sin^2\chi_d\sin^2\chi_a]+\mathcal{A}_0^{(2)}(-\gamma_{202}t_{ef}P_2(\cos\chi_d)-\gamma_{022}t_{ie}P_2(\cos\chi_a)$$
$$+\gamma_{222}t_{ie}t_{ef}[\tfrac{4}{3}P_2(\cos\chi_d)P_2(\cos\chi_a)+\sin^2\chi_d\sin^2\chi_a])+\mathcal{A}_0^{(4)}\gamma_{224}t_{ie}t_{ef}[8P_2(\cos\chi_d)P_2(\cos\chi_a)-\sin^2\chi_d\sin^2\chi_a]\}. \tag{19}$$

The same expression applies also to the coaxially probed geometry [Fig. 2(b)] when $P_2(\cos\chi_a)$ is replaced by $-\frac{1}{2}$ and $\sin^2\chi_a$ is replaced by $-\cos 2\chi_a$ (see Table I).

The five coefficients $\gamma_{k_d k_a k}$ appearing in Eq. (19) attain simple values in the high-J_i limit. The $6j$- and $9j$- coefficients in Eq. (9) can be evaluated in this limit using Eqs. (3.18) and (3.22) of CMH.[7] Taking as well the high-J_i limits of the $b^{(k)}(J_i)$ factors of Eqs. (10)–(12) we find that when $J_i\to\infty$

$$\gamma_{220}=\tfrac{3}{20},\quad \gamma_{202}=\tfrac{1}{2},\quad \gamma_{022}=\tfrac{1}{2},\quad \gamma_{222}=\tfrac{3}{28},\quad \gamma_{224}=\tfrac{9}{140}. \tag{20}$$

Thus in the high-J_i limit the fluorescence intensity assumes the form for the mutually orthogonal geometry:

$$I(\chi_d,\chi_a)=\frac{CS}{9(2J_i+1)(2J_e+1)}\{1+\tfrac{3}{20}t_{ie}t_{ef}[\tfrac{4}{3}P_2(\cos\chi_d)P_2(\cos\chi_a)-\sin^2\chi_d\sin^2\chi_a]+\mathcal{A}_0^{(2)}(-\tfrac{1}{2}t_{ef}P_2(\cos\chi_d)-\tfrac{1}{2}t_{ie}P_2(\cos\chi_a)$$
$$+\tfrac{3}{28}t_{ie}t_{ef}[\tfrac{4}{3}P_2(\cos\chi_d)P_2(\cos\chi_a)+\sin^2\chi_d\sin^2\chi_a])+\mathcal{A}_0^{(4)}\tfrac{9}{140}t_{ie}t_{ef}[8P_2(\cos\chi_d)P_2(\cos\chi_a)-\sin^2\chi_d\sin^2\chi_a]\}. \tag{21}$$

Once again, the result for the coaxially probed geometry is simply obtained from Eq. (21) by replacing $P_2(\cos\chi_a)$ by $-\frac{1}{2}$ and $\sin^2\chi_a$ by $-\cos 2\chi_a$. Equation (21) coincides with the LIF intensity expression derived in Ref. 8 in the case of a $Q\uparrow Q\downarrow$ transition; the Legendre moments a_k of Ref. 8 are related to ours by $\mathcal{A}_0^{(2)}=\frac{2}{5}a_2$ and $\mathcal{A}_0^{(4)}=\frac{1}{9}a_4$.

Because of the structure of the branch parameters t_{ie} and t_{ef} [see Eq. (18)], for the same degree of alignment the polarization of laser-induced fluorescence is two to four times greater for Q than P or R branches. This fact should be considered in designing LIF experiments when it is possible to choose the absorption and emission branches.

Although Eq. (21) has an appealing form, the high-J_i limit may be approached surprisingly slowly in some cases. This behavior is illustrated in Table III which gives the values of $\gamma_{k_d k_a k}$ obtained using the exact results for various branches from Eqs. (1)–(12), showing the typical convergence of the γ's for the nine $J_i\to J_e\to J_f$ resonance fluorescence transitions. Notice the much more rapid convergence for Q branch transitions, particularly $Q\uparrow Q\downarrow$ (20 → 20 → 20) than for those involving purely P and R branch transitions. At $J_i=20$ the typical deviations of $\gamma_{k_d k_a k}$ from the limiting values are, for those involving P and R branches, somewhat larger than 10%, while for the $Q\uparrow Q\downarrow$ transition the deviations are less than 1%. These deviations decrease roughly as $1/J_i$ with increasing J_i. Clearly caution must be exercised in using the high-J_i limit for the LIF intensity expression.

C. Some examples

The simplest nontrivial test case for the LIF intensity expression (1) is a product state with $J_i=2$, as this is the lowest J_i which can support a hexadecapole alignment. As an example we present a complete evaluation of the six terms in Eq. (1) for the transition 2 → 3 → 2 ($J_i=2, J_e=3, J_f=2$; $t_{ie}=1$, $t_{ef}=1$) for a mutually orthogonal geometry:

$$I=\frac{CS}{315}\left\{1+\frac{9}{25}\left[\frac{4}{3}P_2(\cos\chi_d)P_2(\cos\chi_a)-\sin^2\chi_d\sin^2\chi_a\right]+\mathcal{A}_0^{(2)}\left(-\frac{24}{35}P_2(\cos\chi_d)-\frac{2}{7}P_2(\cos\chi_a)\right.\right.$$
$$\left.\left.+\frac{36}{245}\left[\frac{4}{3}P_2(\cos\chi_d)P_2(\cos\chi_a)+\sin^2\chi_d\sin^2\chi_a\right]\right)+\mathcal{A}_0^{(4)}\left(\frac{36}{1225}\right)[8P_2(\cos\chi_d)P_2(\cos\chi_a)-\sin^2\chi_d\sin^2\chi_a]\right\}. \tag{22}$$

One way to test Eq. (22) is to suppose that a single pair of magnetic sublevels of the state $|i\rangle$ are populated, say $M_i=\pm 2$. The alignment parameters in this case are obtained from Eqs. (4) and (5): $\mathcal{A}_0^{(2)}=1$; $\mathcal{A}_0^{(4)}=1/24$. If the polarization axis of the incident laser light is set parallel to the axis of quantization ($\chi_a=0°$), then only the $M_e=\pm 2$ states of the excited level will be populated. Relatively simple arguments given for example by FM, show that the linear polarization of the fluorescence from the excited $J_i=3$, $M_i=\pm 2$ levels happens to vanish. [See, e.g., Eq. (20) and Table I of GZ.[2]] Direct evaluation of Eq. (22) at $\chi_a=0$ confirms this, as $I=CS/441$, independently of χ_d. A nonzero polarization of the laser-induced fluorescence is found instead if the state $|i\rangle$ has initially $M_i=0$. This distribution has a quadrupole alignment $\mathcal{A}_0^{(2)}=-1$ and a hexadecapole alignment

TABLE III. Departures of $\gamma_{k_d k_a k}$ from its high-J_i limit for finite J_i.

$J_i \to J_e \to J_f$	γ_{220}	γ_{202}	γ_{022}	γ_{222}	γ_{224}
$J_i \to \infty$	0.1500	0.5000	0.5000	0.1071	0.0643
$20 \to 21 \to 22$	0.1500	0.4651	0.4651	0.0997	0.0508
$20 \to 21 \to 21$	0.1607	0.4983	0.4651	0.1068	0.0544
$20 \to 21 \to 20$[a]	0.1725	0.5348	0.4651	0.1146	0.0584
$20 \to 20 \to 21$	0.1393	0.4618	0.5000	0.1000	0.0598
$20 \to 20 \to 20$	0.1498	0.4964	0.5000	0.1075	0.0643
$20 \to 20 \to 19$	0.1613	0.5346	0.5000	0.1158	0.0692
$20 \to 19 \to 20$	0.1286	0.4616	0.5385	0.0989	0.0709
$20 \to 19 \to 19$	0.1388	0.4980	0.5385	0.1067	0.0765
$20 \to 19 \to 18$	0.1500	0.5384	0.5385	0.1154	0.0827

[a]For $40 \to 41 \to 40$ the corresponding γ's are: $\gamma_{220} = 0.1613$, $\gamma_{202} = 0.5181$, $\gamma_{022} = 0.4819$, $\gamma_{222} = 0.1110$, and $\gamma_{224} = 0.0612$, showing how the approach to the high-J_i limit is roughly as $1/J_i$.

$\mathcal{A}_0^{(4)} = 1/4$. Taking the laser polarization again to lie along $\hat{z}$ ($\chi_a = 0$) the linear polarization of the emitted light is found using Eq. (22) to be $P = 1/2$, again in agreement with simple arguments. Comparison of Eq. (22) with Eq. (21) shows that the intensity expression at low-J_i values is considerably different from the high-J_i limit.

In LIF studies it is customary to pump a well-defined $J_i - J_e$ transition but not to resolve the subsequent fluorescence. We stress that all the above results apply provided one simply sums Eq. (1) or equivalently Eq. (19) over all final J_f levels (where we assume that the detector has a flat response for the different branches). The only dependence of the LIF intensity I on J_f in Eq. (1) is through the line strength S and the factor $\omega(k_d, k_a, k; J_i J_e, J_f)$. Let us illustrate the case of unresolved detection using the results given in Table III. We assume, e.g., that we are dealing with a ${}^1\Sigma - {}^1\Sigma$ transition whose P and R branch line strengths are J'' and $J'' + 1$, respectively, where J'' is the rotational angular momentum quantum number of the lower level. Then, denoting by $\bar{\gamma}$ the weighted mean value of γt_{ef}, for $P\uparrow$ pumping of the $J_i = 20$ level with unresolved $P\downarrow$ and $R\downarrow$ emission, $\bar{\gamma}_{220} = 0.1390$, $\bar{\gamma}_{202} = 0.4990$, $\bar{\gamma}_{022} = 0.5385$, $\bar{\gamma}_{222} = 0.1069$, and $\bar{\gamma}_{224} = 0.0766$, while for $R\uparrow$ pumping of the same level with unresolved $P\downarrow$ and $R\downarrow$ emission, $\bar{\gamma}_{220} = 0.1610$, $\bar{\gamma}_{202} = 0.4991$, $\bar{\gamma}_{022} = 0.4651$, $\bar{\gamma}_{222} = 0.1070$, and $\bar{\gamma}_{224} = 0.0545$. Although this averaging of the $P\downarrow$ and $R\downarrow$ transitions weighted by their corresponding line strengths does not uniformly improve the convergence to the high-J_i limit, the behavior is more similar to a $Q\uparrow Q\downarrow$ transition. If both the P and R excitation branches are averaged as well, weighted by their line strengths, then $\bar{\bar{\gamma}}_{220} = 0.1503$, $\bar{\bar{\gamma}}_{202} = 0.4991$, $\bar{\bar{\gamma}}_{022} = 0.5009$, $\bar{\bar{\gamma}}_{222} = 0.1070$, and $\bar{\bar{\gamma}}_{224} = 0.0653$, for which each value of $\bar{\bar{\gamma}}$ deviates by no more than 0.2% from the high-J_i limit except $\bar{\bar{\gamma}}_{224}$, which deviates by about 1.5%. More complicated cases of unresolved resonance fluorescence are treated in exactly the same manner provided the necessary line strengths are known.

D. Influence of hyperfine structure

When a reaction product has a nonzero nuclear spin **I**, its coupling with **J** to form a resultant **F** can only lower the observed polarization. Provided $I \ll J_i$, often the case for molecular fragments, this depolarization is negligible. A full treatment of depolarization would be somewhat complicated, because the hyperfine components of the initial state may be excited coherently by the collision process, and the hyperfine components of the excited state may fluoresce coherently. The hyperfine depolarization of fluorescence has been considered previously by FM[1] and discussed qualitatively by GZ.[2] There may be coherence among the hyperfine components of the initial state $|i)$. However this coherence is inconsequential when the time between the birth of the initial state and its absorption of light is long compared to the period of hyperfine precession of **J** about **F**. With this assumption, which is often experimentally realized, each factor $\mathcal{A}^{(k)}$ representing electronic alignment in Eq. (1) is multiplied by

$$\bar{g}^{(k)} = \sum_{F_i} \frac{(2F_i+1)^2}{2I+1} \begin{Bmatrix} F_i & F_i & k \\ J_i & J_i & I \end{Bmatrix}^2 . \tag{23}$$

The parameter $\bar{g}^{(k)}$ is less than unity and its value approaches 1 when $J_i \gg I$. In this limit the squared $6j$-coefficient is approximately given by $[P_k(\hat{J}_i \cdot \hat{F}_i)]^2/(2F_i+1)(2J_i+1)$ and $\bar{g}^{(k)}$ approaches $\sum_{F_i}(2F_i+1)[P_k(\hat{J}_i \cdot \hat{F}_i)]^2/(2J_i+1)(2I+1)$ which equals unity when $\hat{J}_i \cdot \hat{F}_i = 1$. The factor $\bar{g}^{(k)}$ accounts for the effects of hyperfine depolarization in the absorption process only.

The presence of nuclear spin also affects the emission process, even if the hyperfine structure is unresolved by the detection apparatus. This requires that in Eq. (1) each $\omega(k_d, k_a, k; J_i, J_e, J_f)$ is multiplied by

$$\bar{g}^{(k_d)} = \sum_{F_e, F_e'} \frac{(2F_e+1)(2F_e'+1)}{2I+1} \times \begin{Bmatrix} F_e & F_e' & k_d \\ J_e & J_e & I \end{Bmatrix}^2 \frac{1}{1+\omega_{F_e', F_e}^2 \tau^2} , \tag{24}$$

where τ is the radiative lifetime of the state $|e)$ and ω_{F_e', F_e} is the frequency splitting of excited state hyperfine levels. [See Eq. (37) of GZ.[2]] The derivation of this expression assumes that the bandwidth of the light source spans all of the excited state hyperfine components. Note that $\bar{g}^{(0)} = 1$ in both Eqs. (23) and (24), so that the population n_i is not affected by these depolarization factors. In the limit $|\omega_{F_e', F_e}| \ll \tau^{-1}$, essentially no hyperfine precession occurs before the light is emitted and $\bar{g}^{(k_d)} \approx 1$. In the opposite extreme $|\omega_{F_e', F_e}| \gg \tau^{-1}$, many precessions occur before the light is emitted and Eq. (24) reduces to

$$\bar{g}^{(k_d)} \approx \sum_{F_e} \frac{(2F_e+1)^2}{2I+1} \begin{Bmatrix} F_e & F_e & k_d \\ J_e & J_e & I \end{Bmatrix}^2 , \tag{25}$$

which has the structure of Eq. (23). Thus only when J_i is comparable to I must hyperfine depolarization be considered.

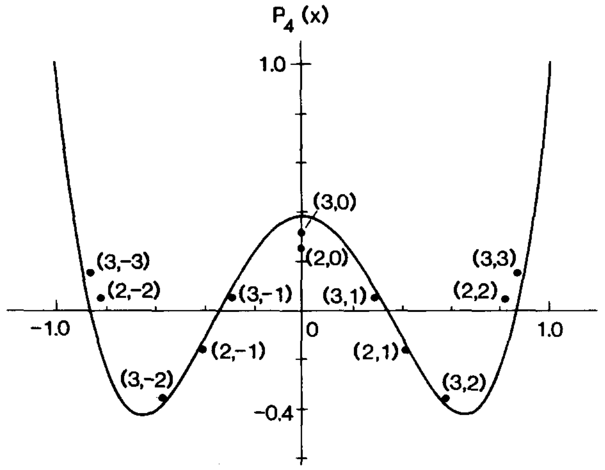

FIG. 4. The Legendre polynomial $P_4(\hat{J}_i \cdot \hat{z})$ and values of $\mathcal{A}_0^{(4)}$ for specific (J_i, M_i) states. We interpret $\hat{J}_i \cdot \hat{z}$ as $M_i/[J_i(J_i+1)]^{1/2}$.

E. Interpretation of the alignment parameters

The values of the alignment parameters $\mathcal{A}_0^{(2)}$ and $\mathcal{A}_0^{(4)}$ provide information on the spatial distribution of the angular momentum vectors $\mathbf{J}_i$ of product molecules. As discussed in GZ[2] $\mathcal{A}_0^{(2)}$ is negative when low M_i ($\ll J_i$) values are primarily excited, implying that $\mathbf{J}_i$ lies predominantly at right angles to the symmetry axis $\hat{z}$. When $\mathbf{J}_i$ lies mainly along $\hat{z}$ and large values of M_i ($\sim J_i$) are excited, $\mathcal{A}_0^{(2)}$ is positive. The analogous interpretation of $\mathcal{A}_0^{(4)}$ is less straightforward. Figure 4 shows $\mathcal{A}_0^{(4)}$ as a function of $\hat{J}_i \cdot \hat{z} = M_i/\sqrt{J_i(J_i+1)}$ in the high-J_i limit where $\mathcal{A}_0^{(4)} = P_4(\mathbf{J}_i \cdot \hat{z})$. This distribution is compared to some exact values of $\mathcal{A}_0^{(4)}$ obtained [from Eq. (5)] if a single (J_i, M_i) state is excited. Already the limiting high-J_i form agrees closely with the exact values for $J_i = 2$ and 3. Positive values of $\mathcal{A}_0^{(4)}$ occur either for $M_i \approx 0$ or $M_i \sim \pm J_i$. Midway between these extremes $\mathcal{A}_0^{(4)}$ is negative. Whereas $\mathcal{A}_0^{(2)}$ primarily relates to the average or most likely value of $\hat{J}_i \cdot \hat{z}$, $\mathcal{A}_0^{(4)}$ can have several effects, one of which is to sharpen or narrow the distribution.

At first it might be thought that $\mathcal{A}_0^{(2)}$ and $\mathcal{A}_0^{(4)}$ are completely independent quantities, but this impression is false when either lies close to one of its extrema; in this situation, the value of the other alignment parameter is constrained. Indeed if one is exactly at an extreme value, all multipole moments of the system are known. (This is a consequence of a joint requirement that the eigenvalues of the density matrix are positive definite and sum to unity.) Let us illustrate this by example. A system which has a quadrupole alignment at its negative extreme $\mathcal{A}_0^{(2)} = -1$ must necessarily be in the pure state $M_i = 0$. For any pure state all multipole moments are fixed. For the above example with $M_i = 0$,

$$\mathcal{A}_0^{(4)} = \tfrac{3}{8} - 3/4J_i(J_i+1). \tag{26}$$

The alignment parameters $\mathcal{A}_0^{(2)}$ and $\mathcal{A}_0^{(4)}$ refer to the spatial distribution of $\mathbf{J}_i$ [see Eqs. (4) and (5)]. However, in many molecular systems $\mathbf{J}_i$ is the resultant of other angular momenta such as the nuclear rotational angular momentum $\mathbf{N}$ and the electron spin $\mathbf{S}$, i.e., $\mathbf{J} = \mathbf{N} + \mathbf{S}$, in Hund's case (b) molecules in arbitrary Λ states. Then it is often of interest to determine the degree of alignment of the molecule's nuclear rotation. This is a separate problem whose consideration will be deferred.

III. DERIVATION OF THE LIF INTENSITY USING A FANO-MACEK-TYPE TREATMENT

As in the formulation of impact-excited fluorescence polarization by Fano and Macek, we begin from an elementary expression for the LIF intensity I and use recoupling algebra to express I in terms of expectation values of angular momentum operators. The problem of laser-induced fluorescence is more complicated than that treated by FM,[1] since *two* photons are involved here. The ability to sort out the geometrical and dynamical aspects of LIF despite this greater complexity illustrates the power of the Wigner–Racah recoupling algebra.

The starting expression for the intensity of a fluorescence transition $J_e \to J_f$ following the resonant absorption process $J_i \to J_e$ is

$$I = C \sum_{M_f} \left\langle \left| \sum_{M_e} (f|\hat{\epsilon}_d \cdot \mathbf{r}|e)(e|\hat{\epsilon}_a \cdot \mathbf{r}|i) \right|^2 \right\rangle . \tag{27}$$

Here $\hat{\epsilon}_d$ and $\hat{\epsilon}_a$ are the polarization unit vectors of the detected photon and the absorbed photon, respectively, and $\mathbf{r}$ represents the dipole moment operator of the molecule. The constant C is proportional to the total population n_i of the initial product state $|i)$ and contains various normalization factors irrelevant to our analysis. It should be noted, however, that when I is expressed as a power flux, C varies with the frequencies of the absorbed (ν_{ie}) and detected (ν_{ef}) photons according to $C \propto \nu_{ie}\nu_{ef}$ (Ref. 4). The summation over M_e in Eq. (27) is coherent because the various alternative paths $M_i \to M_e \to M_f$ for different M_e are indistinguishable. Finally, the brackets $\langle\ \rangle$ indicate an averaging over the distribution of initial state magnetic quantum numbers M_i. The *form* of Eq. (27) is dictated solely by *geometry*, i.e., by the dipole nature of the absorbed and emitted light, and by the fact that no observation is made of the final state $|f)$. The information about the dynamics of the reaction which populates the state $|i)$ is instead reflected solely by the process of *averaging* over M_i. This averaging process is discussed in somewhat greater detail on p. 129 of GZ.[2]

On expanding the absolute square in Eq. (27), the coherence in M_e produces another summation, over the magnetic quantum numbers M_e':

$$I = C \sum_{M_e', M_f, M_e} \langle (i|\hat{\epsilon}_a^* \cdot \mathbf{r}_1|e')(e'|\hat{\epsilon}_d^* \cdot \mathbf{r}_2|f) \times (f|\hat{\epsilon}_d \cdot \mathbf{r}_3|e)(e|\hat{\epsilon}_a \cdot \mathbf{r}_4|i)\rangle . \tag{28}$$

The four dipole operators $\mathbf{r}$ have been labeled here with subscripts 1 through 4 for purposes of bookkeeping in the recoupling algebra to follow, and also to serve as a reminder that the $\mathbf{r}_i$ are independent quantities appearing in separate matrix elements.

An essential step in sorting out the tensorial structure of Eq. (28) is the recognition that the projection operators

$$P_{e'}=\sum_{M_e'}|e')(e'|\ ,$$
$$P_f=\sum_{M_f}|f)(f|\ ,\quad \text{and } P_e=\sum_{M_e}|e)(e| \tag{29}$$

are all scalars (tensors of rank $k=0$). Accordingly we write Eq. (28) in the symbolic form

$$I=C\langle\langle i|(\hat{\epsilon}_a^*\cdot\mathbf{r}_1)P_{e'}(\hat{\epsilon}_d^*\cdot\mathbf{r}_2)P_f(\hat{\epsilon}_d\cdot\mathbf{r}_3)P_e(\hat{\epsilon}_a\cdot\mathbf{r}_4)|i\rangle\rangle\ . \tag{30}$$

The main properties of this intensity expression are difficult to see at a glance, as the polarization vectors $\hat{\epsilon}$ and dipole operators $\mathbf{r}$ are intertwined in a complicated fashion. The first task of recoupling algebra is to reorganize this expression so that all polarization vectors are coupled into one resultant which can then be taken outside of all the matrix elements, and so that all dipole operators are similarly coupled into another resultant. The tensorial notation of Fano and Racah proves useful here. (See especially p. 103 and p. 146 of Judd[21] for examples of this procedure.) Each factor of the operator

$$Q=(\hat{\epsilon}_a^*\cdot\mathbf{r}_1)(\hat{\epsilon}_d^*\cdot\mathbf{r}_2)(\hat{\epsilon}_d\cdot\mathbf{r}_3)(\hat{\epsilon}_a\cdot\mathbf{r}_4) \tag{31}$$

can be represented by the alternative form

$$\hat{\epsilon}\cdot\mathbf{r}=-\sqrt{3}\,[\epsilon^{(1)}\times r^{(1)}]_0^{(0)}$$
$$\equiv-\sqrt{3}\sum_{qq'}\epsilon_q^{(1)}r_{q'}^{(1)}(1q,1q'|00)\ . \tag{32}$$

Here each vector is written in terms of its spherical components, e.g., $\epsilon_0^{(1)}=\epsilon_z$, $\epsilon_{\pm1}^{(1)}=(\mp\epsilon_x-i\epsilon_y)/\sqrt{2}$, and the proportionality factor $-\sqrt{3}$ is required to make Eq. (32) hold identically. Treating the two "d" factors in Eq. (31) first, we write them as

$$(\hat{\epsilon}_d^*\cdot\mathbf{r}_2)(\hat{\epsilon}_d\cdot\mathbf{r}_3)=3\{[\epsilon_d^{*(1)}\times r_2^{(1)}]^{(0)}\times[\epsilon_d^{(1)}\times r_3^{(1)}]^{(0)}\}_0^{(0)}$$
$$=3\sum_{k_d}\{[\epsilon_d^{*(1)}\times\epsilon_d^{(1)}]^{(k_d)}\times[r_2^{(1)}\times r_3^{(1)}]^{(k_d)}\}_0^{(0)}$$
$$\times((11)k_d(11)k_d|(11)0(11)0)^{(0)}\ . \tag{33}$$

In the last step the four unit angular momenta have been recoupled using Eq. (12.11) of FR,[6] or Eq. (3.9) of Rotenberg *et al.*[15] The transformation coefficient involves a $9j$ coefficient with three zeroes and can be evaluated explicitly:

$$((11)k_d(11)k_d|(11)0(11)0)^{(0)}=\tfrac{1}{3}(2k_d+1)^{1/2}\ . \tag{34}$$

Physically, the factor $[\epsilon_d^{*(1)}\times\epsilon_d^{(1)}]^{(k_d)}$ is interpreted as a 2^{k_d} multipole moment of the emitted (i.e., detected) radiation, where $k_d=0$, 1, or 2. After an analogous recoupling to form the multipole moments of rank k_a of the absorbed radiation, the operator Q in Eq. (31) looks like

$$\sum_{k_a,k_d}[\{[\epsilon_d^{*(1)}\times\epsilon_d^{(1)}]^{(k_d)}\times[r_2^{(1)}\times r_3^{(1)}]^{(k_d)}\}^{(0)}$$
$$\times\{[\epsilon_a^{*(1)}\times\epsilon_a^{(1)}]^{(k_a)}\times[r_1^{(1)}\times r_4^{(1)}]^{(k_a)}\}^{(0)}]_0^{(0)}$$
$$\times(2k_d+1)^{1/2}(2k_a+1)^{1/2}\ . \tag{35}$$

With one more recoupling transformation all of the polarization factors can be grouped together as desired,

$$Q=\sum_{k_d,k_a,k}[\{[\epsilon_d^{*(1)}\times\epsilon_d^{(1)}]^{(k_d)}\times[\epsilon_a^{*(1)}\times\epsilon_a^{(1)}]^{(k_a)}\}^{(k)}$$
$$\times\{[r_2^{(1)}\times r_3^{(1)}]^{(k_d)}\times[r_1^{(1)}\times r_4^{(1)}]^{(k_a)}\}^{(k)}]_0^{(0)}$$
$$\times(2k_d+1)^{1/2}(2k_a+1)^{1/2}((k_dk_a)k(k_dk_a)k|(k_dk_d)0(k_ak_a)0)^{(0)}\ . \tag{36}$$

Using the relation

$$((k_dk_a)k(k_dk_a)k|(k_dk_d)0(k_ak_a)0)^{(0)}$$
$$=(2k+1)^{1/2}(2k_d+1)^{-1/2}(2k_a+1)^{-1/2} \tag{37}$$

and the scalar product

$$[F^{(k)}\times G^{(k)}]_0^{(0)}=\sum_q(-1)^{k-q}F_q^{(k)}G_{-q}^{(k)}(2k+1)^{-1/2}\ , \tag{38}$$

we finally have the key result

$$Q=\sum_{k_d,k_a,k,q}(-1)^{k-q}\{[\epsilon_d^{*(1)}\times\epsilon_d^{(1)}]^{(k_d)}\times[\epsilon_a^{*(1)}\times\epsilon_a^{(1)}]^{(k_a)}\}_q^{(k)}$$
$$\times\{[r_2^{(1)}\times r_3^{(1)}]^{(k_d)}\times[r_1^{(1)}\times r_4^{(1)}]^{(k_a)}\}_{-q}^{(k)}\ . \tag{39}$$

The indices k and q, with $|k_d-k_a|\le k\le k_d+k_a$ and $-q\le k\le q$, are net multipole quantum numbers for the combination of absorbed and emitted radiations.

We may now extract the polarization factors from the matrix elements in Eq. (39), obtaining

$$I=C\sum_{k_d,k_a,k,q}(-1)^{k-q}\epsilon(k_d,k_a,k,q;\Omega)\,\langle\langle i|\{[r_2^{(1)}\times r_3^{(1)}]^{(k_d)}$$
$$\times[r_1^{(1)}\times r_4^{(1)}]^{(k_a)}\}_{-q}^{(k)}P_{e'}P_fP_e|i\rangle\rangle\ , \tag{40}$$

where we have defined the *polarization tensors* by

$$\epsilon(k_d,k_a,k,q;\Omega)=\{[\epsilon_d^{*(1)}\times\epsilon_d^{(1)}]^{(k_d)}$$
$$\times[\epsilon_a^{*(1)}\times\epsilon_a^{(1)}]^{(k_a)}\}_q^{(k)}\ . \tag{41}$$

The operator in the expectation value (40) is a rank k tensor ($0\le k\le 4$) operating on the initial state only, with the dependence on J_e and J_f embodied in the projection operators $P_{e'}$, P_f, and P_e. Using the Wigner–Eckart theorem, we now replace this complicated tensor operator by the angular momentum operator $J_{-q}^{(k)}$. This replacement introduces a compensating ratio of reduced matrix elements

$$I=\sum_{k_d,k_a,k,q}(-1)^{k-q}\epsilon(k_d,k_a,k,q;\Omega)\langle\langle i|J_{-q}^{(k)}|i\rangle\rangle$$
$$\times(J_i\|\{[r_2^{(1)}\times r_3^{(1)}]^{(k_d)}\times[r_1^{(1)}\times r_4^{(1)}]^{(k_a)}\}^{(k)}$$
$$\times P_{e'}P_fP_e\|J_i)/(J_i\|J^{(k)}\|J_i)\ . \tag{42}$$

The operator $J_q^{(k)}$ is the same angular momentum operator as given by Biedenharn,[22] with $J_k^{(k)}=[2^{-1/2}(-J_x-iJ_y)]^k$ and with the remaining elements $J_q^{(k)}$ obtained from the commutation relations with J:

$$[J_z,J_q^{(k)}]=qJ_q^{(k)}\ ;$$
$$[J_\pm,J_q^{(k)}]=[k(k+1)-q(q\pm1)]^{1/2}J_{q\pm1}^{(k)}\ . \tag{43}$$

The only elements we require for the cylindrically symmetric problem here are those with $q=0$, and when the reacting particles have no net spin helicity or chirality the odd k terms vanish also. The relevant operators are thus

$$J_0^{(0)}=1\ ;\quad J_0^{(2)}=(3J_z^2-\mathbf{J}^2)/\sqrt{6}\ ;$$
$$J_0^{(4)}=(3\mathbf{J}^4-6\mathbf{J}^2-30J_z^2\mathbf{J}^2+25J_z^2+35J_z^4)/2\sqrt{70}\ . \tag{44}$$

To obtain dynamical parameters with simple ranges of variations, it is useful to introduce renormalized alignment parameters $\mathcal{A}_q^{(k)}$, where

$$\mathcal{A}_0^{(0)}=1\ ;\quad \mathcal{A}_0^{(2)}=\langle (i|J_0^{(2)}|i)\rangle\sqrt{6}/J_i(J_i+1)\ ;$$
$$\mathcal{A}_0^{(4)}=\langle (i|J_0^{(4)}|i)\rangle\sqrt{70}/4J_i^2(J_i+1)^2\ . \tag{45}$$

These have simple ranges of variation, as discussed in Sec. II. The reduced matrix elements of the angular momentum operators are straightforward to evaluate. In terms of the well-known matrix elements of J_+ and Clebsch–Gordan coefficients they are given by

$$(J_i\|J^{(k)}\|J_i)=\frac{(-1)^k\sqrt{2J_i+1}\,(J_i,k-J_i|J_+^k|J_i,-J_i)}{2^{k/2}(J_i,k-J_i|J_i-J_i,kk)}\ , \tag{46}$$

using the conventions of Messiah.[23] More explicitly,

$$(J_i\|J^{(0)}\|J_i)=(2J_i+1)^{1/2}\ ,$$
$$(J_i\|J^{(2)}\|J_i)=[J_i(J_i+1)(2J_i+3)(2J_i+1)(2J_i-1)/6]^{1/2}\ ,$$
$$(J_i\|J^{(4)}\|J_i)=[(J_i-1)J_i(J_i+1)(J_i+2)(2J_i+5)(2J_i+3)\times(2J_i+1)(2J_i-1)(2J_i-3)/70]^{1/2}\ , \tag{47}$$

which differ from those tabulated in CMH[7] by a factor $(2J_i+1)^{1/2}$ owing to a difference in conventions. It will also prove useful to define a rescaling factor $b^{(k)}(J_i)$ by the equation

$$\mathcal{A}_0^{(k)}b^{(k)}(J_i)=\langle (i|J_0^{(k)}|i)\rangle/(J_i\|J^{(k)}\|J_i)\ . \tag{48}$$

The factors $b^{(k)}(J_i)$ were already given in Eqs. (10)–(12) above.

The last factor to evaluate in Eq. (42) is the radial reduced matrix element. It can be written in a complicated but more detailed form as

$$(J_i\|\{[r_2^{(1)}\times r_3^{(1)}]^{(k_d)}\times[r_1^{(1)}\times r_4^{(1)}]^{(k_a)}\}^{(k)}P_{e'}P_fP_e\|J_i)=\sum_{\text{all }M,q}(J_iM_i|r_{q_1}^{(1)}|J_eM_{e'})(J_eM_{e'}|r_{q_2}^{(1)}|J_fM_f)$$
$$\times(J_fM_f|r_{q_3}^{(1)}|J_eM_e)(J_eM_e|r_{q_4}^{(1)}|J_iM_{i'})(1q_2,1q_3|k_dq_d)(1q_1,1q_4|k_aq_a)(k_dq_d,k_aq_a|kq)(-1)^{J_i-M_i}\begin{pmatrix}J_i & k & J_i\\ -M_i & q & M_{i'}\end{pmatrix}\ . \tag{49}$$

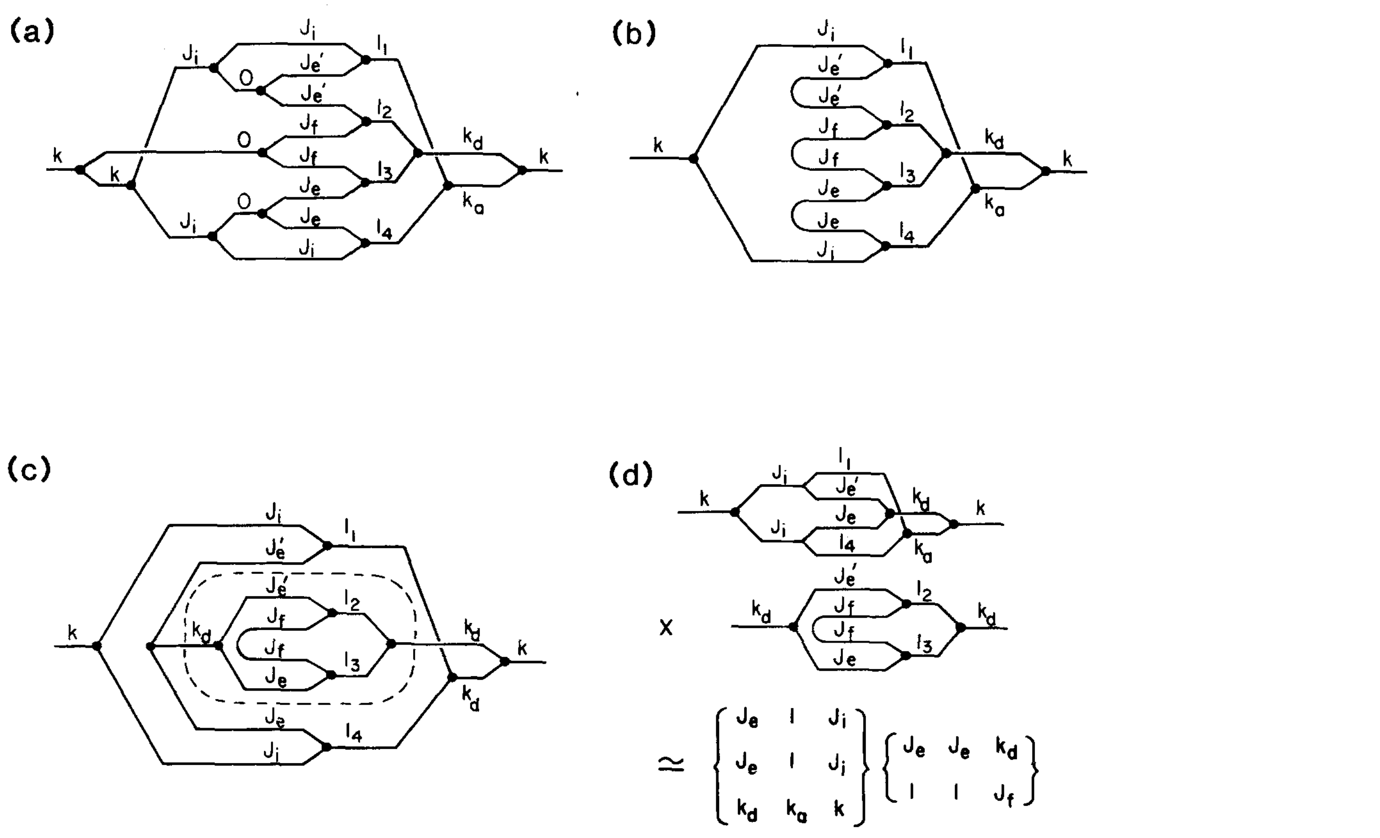

FIG. 5. Angular momentum coupling diagram relevant for the evaluation of the reduced matrix element in Eq. (49). Its dependence on angular momentum quantum numbers should be given, in essence, by the 21j coefficient having three vanishing angular momenta, shown in Fig. 5(a). Note that an nj coefficient has $(2n/3)$ nodes. By erasing all lines with zeroes, the 12j coefficient shown in Fig. 5(b) is obtained. The lines J_e and J_e' can be "pinched" together by recoupling them into a resultant k_d'. In general this involves a summation over all possible values of k_d'. One portion of the diagram is connected to the rest by only two lines k_d' and k_d, picking out only a single term with $k_d'=k_d$. This portion is shown inside the closed dashed line in Fig. 5(c). Finally, a slight rearrangement gives the 12j coefficient as a product of a 9j coefficient and a 6j coefficient, shown in Fig. 5(d).

After applying the Wigner–Eckart theorem to the radial matrix elements in Eq. (49), we are left with a summation over eight $3j$ coefficients. As a guide to the explicit evaluation of this summation, we have found graphical techniques useful. This approach is outlined in Fig. 5. Qualitatively, we expect the dependence of this reduced matrix element on J_i, J_e, J_f, k_d, k_a, and k to be given by the projection of a state whose coupling scheme is

$$|[(J_{e'}J_f)1_2(J_fJ_e)1_3]k_d[(J_iJ_{e'})1_1(J_eJ_i)1_4]k_a\rangle^{(k)} \tag{50}$$

[i.e., the right-hand half of Fig. 5(a)] onto a second state in which $P_{e'}$, P_f, and P_e are forced to be scalars:

$$\langle\{[J_i(J_{e'}J_{e'})0]J_i[(J_eJ_e)0J_i]J_i\}k(J_fJ_f)0|^{(k)} , \tag{51}$$

[the left-hand half of Fig. 5(a)]. This recoupling transformation amounts to a $21j$ coefficient with three zeroes. As discussed in the caption to Fig. 5, this matrix element factorizes into the product of a $6j$ and a $9j$ coefficient

$$\text{Fig. } 5 \propto \begin{Bmatrix} J_e & J_e & k_d \\ 1 & 1 & J_f \end{Bmatrix} \begin{Bmatrix} J_e & 1 & J_i \\ J_e & 1 & J_i \\ k_d & k_a & k \end{Bmatrix} , \tag{52}$$

which contains the essential factors in the reduced matrix element. (Here we have dropped the primes and subscripts which we had used for labeling.) Diagrammatic methods have served us as a "roadmap" in the algebraic evaluation of the radial reduced matrix element. As suggested by Fig. 5, the first step is the completion of the summation over M_f using Eq. (2.19) of Rotenberg *et al.*,[15] giving the $6j$ coefficient in Eq. (52), after which Eq. (3.1) of Ref. 15 contributes the $9j$ coefficient. In general complicated phase factors enter the final result, but restricting ourselves to even values of k_d, k_a, and k we find

$$\begin{aligned}(J_i\|\{[r_2^{(1)}\times r_3^{(1)}]^{(k_d)}\times[r_1^{(1)}\times r_4^{(1)}]^{(k_a)}\}^{(k)}P_{e'}P_fP_e\|J_i)\\ =S(J_i,J_e,J_f)h(k_d,k_a,k;J_i,J_e,J_f) ,\end{aligned} \tag{53}$$

where the product of absorption and emission line strengths is

$$S(J_i,J_e,J_f)=|(J_f\|r^{(1)}\|J_e)(J_e\|r^{(1)}\|J_i)|^2 \tag{54}$$

and the factor h is

$$\begin{aligned}h(k_d,k_a,k;J_i,J_e,J_f)&=(-1)^{J_e+J_f+1}(2k_d+1)^{1/2}(2k_a+1)^{1/2}\\ &\times(2k+1)^{1/2}\begin{Bmatrix} J_e & J_e & k_d \\ 1 & 1 & J_f \end{Bmatrix} \begin{Bmatrix} J_e & 1 & J_i \\ J_e & 1 & J_i \\ k_d & k_a & k \end{Bmatrix} .\end{aligned} \tag{55}$$

This completes the derivation of Eqs. (1)–(12) above.

ACKNOWLEDGMENTS

We thank R. N. Dixon, U. Fano, and C. T. Rettner for useful comments.

APPENDIX: CALCULATION OF THE POLARIZATION TENSORS

The polarization tensors are linear combinations of components of the polarization unit vectors $\hat{\epsilon}_d$ and $\hat{\epsilon}_a$ describing the detected and absorbed radiations. They have a simple general form in a primed coordinate frame whose $\hat{z}'$ axis coincides with the photon propagation axis. In the "detected photon" coordinate frame, e.g., the detected photon polarization vector can be written as $\hat{\epsilon}_d=(\cos\beta_d, i\sin\beta_d, 0)$, where β_d specifies the elliptical polarization of the light.[1] Light which is linearly polarized along the $\hat{x}'$ axis is then represented by $\beta_d=0$, while circularly polarized light with a positive (or negative) component of angular momentum along the propagation axis $\hat{z}'$ has $\beta_d=\frac{1}{4}\pi$ (or $-\frac{1}{4}\pi$). Since there is no uniform convention for defining left-hand and right-hand circularly polarized light in the literature, we refer instead to circularly polarized light being positive or negative. (In GZ[2] we called the positive helicity left-hand circularly polarized.) Similarly, in the "absorbed photon" coordinate frame the absorbed photon polarization vector is $\hat{\epsilon}_a=(\cos\beta_a, i\sin\beta_a, 0)$.

In the detection coordinate system the nonvanishing elements of $[\epsilon_d^{*(1)}\times\epsilon_d^{(1)}]_{q_d}^{(k_d)}$ are:

$$\begin{aligned}&[\epsilon_d^{*(1)}\times\epsilon_d^{(1)}]_0^{(0)}=-\frac{1}{\sqrt{3}} , \quad [\epsilon_d^{*(1)}\times\epsilon_d^{(1)}]_0^{(1)}=-\frac{1}{\sqrt{2}}\sin 2\beta_d ,\\ &[\epsilon_d^{*(1)}\times\epsilon_d^{(1)}]_0^{(2)}=-\frac{1}{\sqrt{6}} , \quad [\epsilon_d^{*(1)}\times\epsilon_d^{(1)}]_{\pm2}^{(2)}=\tfrac{1}{2}\cos 2\beta_d ,\end{aligned} \tag{A1}$$

and identical expressions apply to the absorbed photon in the absorption coordinate frame with the substitution $d\to a$. Before we can couple the "d" and "a" factors to form $\epsilon(k_d,k_a,k,q;\Omega)$, they must be transformed into a common coordinate system, which we take to be the "collision frame" whose $\hat{z}$ axis coincides with the collision symmetry axis. This frame transformation involves two sets of Euler angles: (ϕ_d,θ_d,χ_d) which rotate the collision frame (xyz) into the detection frame $(x_d'y_d'z_d')$, and (ϕ_a,θ_a,χ_a) which rotate the collision frame into the absorption frame $(x_a'y_a'z_a')$. We define these angles as in Messiah,[23] whereby the polar coordinates of $\hat{z}_d'$ with respect to the axes (xyz) are (θ_d,ϕ_d) and the polar coordinates of $\hat{z}$ with respect to the axes $(x_d'y_d'z_d')$ are $(\theta_d,\pi-\chi_d)$. When $\hat{z}$ and $\hat{z}_d'$ are parallel we must complement this definition by taking $\phi_d=0$, $\theta_d=0$ and χ_d as the angle between $\hat{x}$ and $\hat{x}_d'$. The same convention also defines (ϕ_a,θ_a,χ_a). For definiteness these Euler angles are taken within the ranges

$$0\le\phi\le2\pi , \quad 0\le\theta\le\pi , \quad -\pi\le\chi\le\pi . \tag{A2}$$

The collision frame tensors are then derived from the relation

$$T_{q_d}^{(k_d)}(\text{col})=\sum_{q_d'}T_{q_d'}^{(k_d)}(\text{det})[D^{(k_d)}(\phi_d,\theta_d,\chi_d)]^{-1}_{q_d',q_d} \tag{A3}$$

also valid with $d\to a$. Because Sec. II considers even $\{k_d,k_a,k\}$, we give the transformed tensors only for them:

$$[\epsilon_d^{*(1)}\times\epsilon_d^{(1)}]_0^{(0)}=-\frac{1}{\sqrt{3}} , \quad [\epsilon_d^{*(1)}\times\epsilon_d^{(1)}]_0^{(2)}=-\frac{1}{\sqrt{6}}[P_2(\cos\theta_d)-\tfrac{3}{2}\cos2\beta_d\sin^2\theta_d\cos2\chi_d] ,$$

$$[\epsilon_d^{*(1)} \times \epsilon_d^{(1)}]_{\pm 1}^{(2)} = \exp(\pm i\phi_d)\{\pm \tfrac{1}{4}\sin 2\theta_d + \tfrac{1}{2}\cos 2\beta_d \sin\theta_d[i\sin 2\chi_d \pm \cos\theta_d\cos 2\chi_d]\} ,$$
$$[\epsilon_d^{*(1)} \times \epsilon_d^{(1)}]_{\pm 2}^{(2)} = \exp(\pm 2i\phi_d)\{-\tfrac{1}{4}\sin^2\theta_d + \tfrac{1}{8}\cos 2\beta_d[(3+\cos 2\theta_d)\cos 2\chi_d \pm 4i\cos\theta_d \sin 2\chi_d]\} , \tag{A4}$$

which are again valid with $d \to a$. Lastly we must couple d to a according to

$$\epsilon(k_d, k_a, k, q; \Omega) = \sum_{q_d, q_a} [\epsilon_d^{*(1)} \times \epsilon_d^{(1)}]_{q_d}^{(k_d)} [\epsilon_a^{*(1)} \times \epsilon_a^{(1)}]_{q_a}^{(k_a)} (k_d q_d, k_a q_a | kq) . \tag{A5}$$

The values of the polarization tensors of interest are then

$$\epsilon(0,0,0,0;\Omega) = \tfrac{1}{3} , \quad \epsilon(2,0,2,0;\Omega) = \frac{1}{3\sqrt{2}}[P_2(\cos\theta_d) - \tfrac{3}{2}\cos 2\beta_d \sin^2\theta_d \cos 2\chi_d] ,$$
$$\epsilon(0,2,2,0;\Omega) = \frac{1}{3\sqrt{2}}[P_2(\cos\theta_a) - \tfrac{3}{2}\cos 2\beta_a \sin^2\theta_a \cos 2\chi_a] , \quad \epsilon(2,2,0,0;\Omega) = \frac{1}{\sqrt{5}}(Q_0 - Q_1 + Q_2) ,$$
$$\epsilon(2,2,2,0;\Omega) = \frac{1}{\sqrt{14}}(-2Q_0 + Q_1 + 2Q_2) , \quad \epsilon(2,2,4,0;\Omega) = \frac{1}{\sqrt{70}}(6Q_0 + 4Q_1 + Q_2) , \tag{A6}$$

where the Q_m are given by

$$Q_0 = \tfrac{1}{6}[P_2(\cos\theta_d) - \tfrac{3}{2}\cos 2\beta_d \sin^2\theta_d\cos 2\chi_d][P_2(\cos\theta_a) - \tfrac{3}{2}\cos 2\beta_a \sin^2\theta_a \cos 2\chi_a] ;$$
$$Q_1 = -\tfrac{1}{2}\cos\phi_{da}[\tfrac{1}{4}\sin 2\theta_d \sin 2\theta_a(1+\cos 2\beta_d\cos 2\chi_d)(1+\cos 2\beta_a \cos 2\chi_a) + \cos 2\beta_d \cos 2\beta_a \sin\theta_d \sin\theta_a \sin 2\chi_d \sin 2\chi_a]$$
$$+ \tfrac{1}{4}\sin\phi_{da}[\cos 2\beta_d \sin\theta_d \sin 2\chi_d \sin 2\theta_a(1+\cos 2\beta_a\cos 2\chi_a) - \cos 2\beta_a \sin\theta_a \sin 2\chi_a \sin 2\theta_d(1+\cos 2\beta_d \cos 2\chi_d)] ;$$
$$Q_2 = \tfrac{1}{8}\cos 2\phi_{da}\{[\sin^2\theta_d - \cos 2\beta_d(1+\cos^2\theta_d)\cos 2\chi_d][\sin^2\theta_a - \cos 2\beta_a(1+\cos^2\theta_a)\cos 2\chi_a]$$
$$+ \cos 2\beta_d \cos 2\beta_a \cos\theta_d \cos\theta_a \sin 2\chi_d \sin 2\chi_a\} + \tfrac{1}{4}\sin 2\phi_{da}\{\cos 2\beta_d \cos\theta_d \sin 2\chi_d$$
$$\times[\sin^2\theta_a - \cos 2\beta_a(1+\cos^2\theta_a)\cos 2\chi_a] - \cos 2\beta_a \cos\theta_a \sin 2\chi_a[\sin^2\theta_d - \cos 2\beta_d(1+\cos^2\theta_d)\cos 2\chi_d]\} . \tag{A7}$$

Here $\phi_{da} = \phi_d - \phi_a$ is the difference between the azimuthal angles of the detected and absorbed photons. The expressions given in Table I for the mutually orthogonal geometry with linearly polarized excitation and detection are recovered upon setting $\beta_d = \beta_a = 0$, $\theta_d = \theta_a = \tfrac{1}{2}\pi$, and $\phi_{da} = \pm\tfrac{1}{2}\pi$, and for the coaxially probed geometry upon setting $\beta_d = \beta_a = 0$, $\theta_d = \tfrac{1}{2}\pi$, $\theta_a = 0$, and $\phi_{da} = \pm \tfrac{1}{2}\pi$.

[1] U. Fano and J. H. Macek, Rev. Mod. Phys. **45**, 553 (1973).
[2] C. H. Greene and R.N. Zare, Annu. Rev. Phys. Chem. **33**, 119 (1982).
[3] R. N. Zare and P. J. Dagdigian, Science **185**, 739 (1974).
[4] J. L. Kinsey, Annu. Rev. Phys. Chem. **28**, 349 (1975).
[5] M. A. A. Clyne and I. S. McDermid, in *Dynamics of the Excited State*, edited by K. P. Lawley (Wiley, New York, 1982), pp. 1–104.
[6] U. Fano and G. Racah, *Irreducible Tensorial Sets* (Academic, New York, 1959).
[7] D. A. Case, G.M. McClelland, and D. R. Herschbach, Mol. Phys. **35**, 541 (1978).
[8] M. P. Sinha, C. D. Caldwell, and R. N. Zare, J. Chem. Phys. **61**, 491 (1974).
[9] A. W. Kleyn, A. C. Luntz, and D. J. Auerbach, Phys. Rev. B **25**, 4273 (1982).
[10] I. V. Hertel, in *The Excited State in Chemical Physics*, edited by J. N. McGowan (Wiley, New York, 1981), pp. 341–398; I. V. Hertel and W. Stoll, Adv. At. and Mol. Phys. **13**, 113 (1978).
[11] C. T. Rettner and R. N. Zare, J. Chem. Phys. **77**, 2416 (1982).
[12] S. Stolte, Ber. Bunsenges. Phys. Chem. **86**, 413 (1982).
[13] R. E. Drullinger and R. N. Zare, J. Chem. Phys. **51**, 5532 (1969); **59**, 4225 (1973).
[14] L. Hahn and I. V. Hertel, J. Phys. B **5**, 1995 (1972); M. H. Mittleman, Phys. Rev. A **14**, 1338 (1976).
[15] M. Rotenberg, R. Bivens, N. Metropolis, and J. K. Wooten, Jr., *The 3j- and 6j-Symbols* (MIT, Cambridge, Massachusetts, 1959).
[16] K. Schulten and R. G. Gordon, J. Math. Phys. **16**, 1961, 1971 (1975); Comput. Phys. Commun. **11**, 269 (1976).
[17] P. P. Feofilov, *The Physical Basis of Polarized Emission* (Consultants Bureau, New York, 1961).
[18] R. N. Zare, J. Chem. Phys. **45**, 4510 (1966).
[19] J.-C. Lehmann, in *Les Houches Session XXVII, Frontiers in Laser Spectroscopy*, edited by R. Balian, S. Haroche, and S. Liberman (North–Holland, Amsterdam, 1977).
[20] R. I. Altkorn (private communication).
[21] B. R. Judd, *Angular Momentum Theory for Diatomic Molecules* (Academic, New York, 1975).
[22] L. C. Biedenharn, Ann. Phys. **4**, 104 (1958).
[23] A. Messiah, *Quantum Mechanics* (North–Holland, Amsterdam, 1965), Vol. II, Appendix C.